TIME AND TEMPERATURE-DEPENDENT PROCESSES AFFECTING NEAR THRESHOLD FATIGUE CRACK GROWTH

W. Gerberich*, A. Wright* and M.-J. Lei**

*Chemical Engineering and Materials Science, University of Minnesota, Minneapolis, MN 55455, USA

**Metallurgy Bureau, The First Tractor Plant, Louyang, Henan, China

ABSTRACT

In a series of Fe-base alloys, the importance of low temperature on the effective driving force for fatigue crack growth is delineated. It is shown that both a crack-opening stress intensity factor and an effective stress intensity factor contribute to threshold. Both factors increase substantially as test temperature is reduced from 300 to 123 K.

KEYWORDS

Fatigue thresholds; low temperature; effective stress intensity; opening stress intensity; closure mechanisms; strain-rate sensitivity; strain-hardening exponents; Fe-binary alloys and HSLA steel.

INTRODUCTION

Assume for the moment that there is a ΔK, below which fatigue cracks either do not grow or do so very slowly, in the range of 10^{-11} to 10^{-10} m/cycle. We will define this as ΔK_{th}, the threshold stress intensity. Attempts to construct generalized threshold models in the past have generally failed because the assumptions have neglected many of the important microstructural or microplastiticy phenomena. Whether such theoretical models have been in terms of dislocation emission (Sadananda and Shahinian, 1977; Yokobori and Yokobori, 1982) a Neuber micro-support concept (Weiss and Lal, 1974) or a local strain criterion (Yu and Yan, 1980), they do not encompass a large range of material behavior. Many such theoretical models would predict threshold to be independent of yield strength or grain size even though experimental studies have strongly demonstrated a dependence on both parameters (Masounave and Bailon, 1976). A brief review of such models, as elaborated upon elsewhere (Yokobori and Yokobori, 1982), gives

(Sadananda and Shahinian 1977) $\Delta K_{th} = 2.09\, E\sqrt{b}$; $b = 2.48\text{Å}$ (1a)

(Yokobori and Yokobori, 1982) $\Delta K_{cr} \simeq 0.357\, E\sqrt{b}$; $b = 2.48\text{Å}$ (1b)

(Weiss and Lal, 1974) $$\Delta K_{th} = 0.387\ E\sqrt{\rho^*}\ ;\ \rho^* \simeq 250\text{Å} \quad (1c)$$

(Yu and Yan, 1980) $$\Delta K_{th} \simeq E\varepsilon_f\sqrt{2\pi\rho_{min}}\ ;\ \rho_{min} = 2.48\text{Å} \quad (1d)$$

Here, E and b are modulus of elasticity and Burgers vector in all cases. For Eq. (1c), ρ^* refers to the Neuber micro-support constant and for Eq. (1d), ε_f and ρ_{min} are the tensile fracture ductility and Burgers vector. In all cases ΔK_{th} is the threshold stress intensity as defined but ΔK_{cr} refers to the critical stress intensity for dislocation emission. As discussed by Yokobori and Yokobori (1982), this is only part of the total ΔK_{th}.

To illustrate this, consider some data that have been generated in a seven year program to evaluate grain size, d, and yield strength, σ_{ys}, effect on thresholds in two steels and a series of Fe-binary alloys. The range of parameters included grain sizes from 10 to 120 μm and test temperatures from 123 to 300 K, the later giving a yield strength range of 122 to 827 MPa. Threshold data, as plotted versus $\sigma_{ys}d^{1/2}$ in Fig. 1, are seen to increase regularly with this parameter.

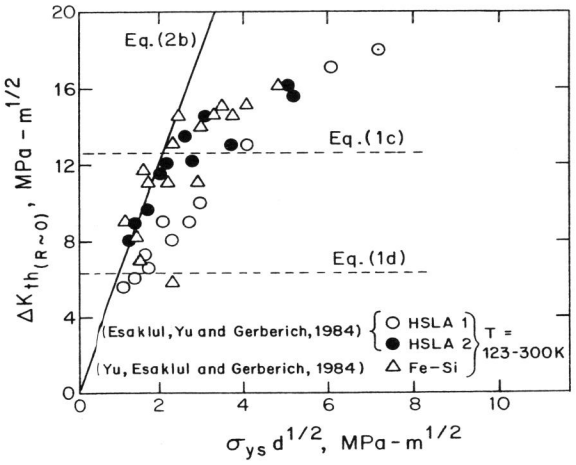

Fig. 1: Effect of combined yield strength, grain size parameter, $\sigma_{ys}d^{1/2}$ on threshold stress intensity. Comparison to theoretical model predictions.

With E = 2.06 x 10^5 MPa and $\varepsilon_f \sim 0.78$, Eqs. (1c) and (1d) are seen to be non-predictive in Fig. 1 as would the other relationships of Eqs. (1). A purely ad hoc assumption that growth rates tend toward zero when the plane strain plastic zone size is equal to the grain size, d, gives

$$R_{p_\pm} \simeq \frac{\Delta K^2_{th(R=0)}}{3\pi(2\sigma_{ys})^2} \sim d \quad (2a) \quad ; \quad \Delta K_{th(R=0)} \simeq 6.14\ \sigma_{ys}\sqrt{d} \quad (2b)$$

Although Eq. (2b) represents the data much better in Fig. 1, this is partly fortuitous since several microscopic phenomena are merged together.

It is the purpose of this paper to separate those microscopic phenomena which operate at low temperatures and contribute to the observed thresholds. First, it is recognized that creep, relaxation, dislocation dynamics and flow stress dependencies may exist at low temperatures near fatigue crack tips. Although this has been investigated over the last eight years (Burck and Weertman, 1976; Yu, Esaklul and Gerberich, 1984), it has only been recently documented that a

large number of synergistic or competing phenomena may contribute to low temperature thresholds (Yu and Gerberich, 1983). The reason for the ambiguity is that threshold is generally made up of two factors, a load to open the crack tip and a further load, just beyond which the crack would take a forward step. Thus, near threshold, the effective stress intensity driving force, ΔK_{eff}, is interpreted in terms of a maximum stress intensity, K_{max}, and an opening stress intensity, K_{op}, to load the crack-tip beyond closure. The usual representation is

$$\Delta K_{eff} = K_{max} - K_{op}\ ;\ K_{op} > K_{min} \quad (3a) \quad ; \quad \Delta K = K_{max}(1-R) \quad (3b)$$

where R is the load ratio, $R = K_{min}/K_{max}$. At threshold, Eqs. (3a), (3b) may be combined to give

$$\Delta K_{th} = (\Delta K_{th(eff)} + K_{op})(1-R) \quad (4)$$

The effective term may involve crack-tip plasticity while the opening term may involve reverse plasticity, surface roughness or oxide closure phenomena. Since threshold is made up of two terms, it is clear that time and low temperature could affect threshold through the crack-tip resistance term (e.g. dislocation emission or cleavage) or the near crack-tip closure term (e.g. the strength or creep of asperities). A partial listing of such effects are provided in Table 1.

In order to better quantify these proposed trends, it is necessary to have detailed measurements of strain-hardening and strain-rate sensitivity exponents, β and m^*, yield stress and K_{op} as a function of test temperature and time (rate). This has been accomplished in large measure on two material systems (Lucas, 1983; Gerberich, Yu and Esaklul, 1984; Esaklul, Yu and Gerberich, 1984).

TABLE 1 Effect of Decreasing Test Temperature or Time

Parameter	Effective Stress Intensity Phenomena	$\Delta K_{th(eff)}$	Closure Phenomena	K_{op}
↑ Yield stress, σ_{ys}	↓ reverse plastic zone size	↑	↑ asperity strength	↑
↑ Strain-rate sensitivity, m^* †	↑ local stress	↓	↓ asperity creep	↑
↓ Strain-hardening exponent, β ††	↑ local strain	↓	↑ reverse plasticity	↑
↑ local flow stress	↑ cyclic cleavage	↓	↑ cleavage asperities	↑
↓ oxidation (e.g. corrosion in relative humidity air)	↑ hydrogen resistance	↑	↓ oxide-induced closure	↓

† $m^* = \partial \ln \dot{\varepsilon}_p / \partial \ln \sigma^*$; †† $\sigma = k\ \varepsilon_p^{\beta}$

RESULTS AND DISCUSSION

Flow Property Relationships at Low Temperature

First, it is useful to demonstrate that flow properties do have a direct but more complex bearing on the threshold behavior typified by the general trends in Fig. 1. Consider crack growth rate veruse ΔK for four Fe-binary alloys at 300 K in Fig. 2(a) and for a high-strength, low-alloy steel at four test temperatures in Fig. 2(b). In the first case, silicon additions decreased threshold and increased growth rates even though they also increased yield strength. In Fig. 2(b), it is seen that lowering test temperature increased threshold and decreased growth rates while also increasing yield strength. The former is not consistent with the general trend in Fig. 1 while the later is. Thus, it is important to understand how alloy additions and test temperature affect the plastic flow parameters in Table 1.

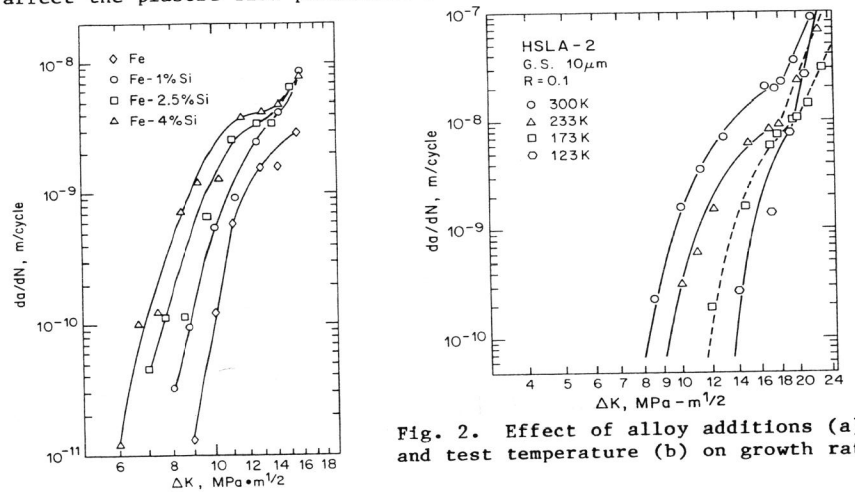

Fig. 2. Effect of alloy additions (a) and test temperature (b) on growth rates.

Interrelationship between Strain Hardening and Strain Rate Sensitivity

Although the interest here is predominantly cyclic stress-strain, it is also possible to apply the present arguments to monotonic stress-strain. Thus to generalize, one accepted form of the cyclic stress-strain curve is given below

$$\frac{\Delta\sigma}{2} = k\left(\frac{\Delta\varepsilon_p}{2}\right)^{\beta_c} \quad \text{or} \quad \sigma_a = k\left(\varepsilon_{ap}\right)^{\beta_c} \tag{5}$$

recognizing that for the monotonic case, the second representation would simply exchange the static strain-hardening exponent, β, for the cyclic one, β_c. It has been recently recognized that Eq. (5) is particularly unsuitable to the understanding of BCC iron-base systems. This has been pointed out by Mughrabi, Herz and Stark (1976) and Lucas and Gerberich (1981) who suggested that the flow stress under cyclic conditions[1] should be partitioned into thermal, $\sigma^*_{(T,\dot{\varepsilon}_p)}$ and athermal, σ_i, components. This is given by

[1] This would apply to monotonic loading as well.

$$\sigma_{(\varepsilon_p)} = \sigma^*_{(T,\dot{\varepsilon}_p)} + \sigma_{i(\varepsilon_p)} \tag{6}$$

which implies that σ^* is only a function of temperature and plastic strain rate and σ_i is only a function of plastic strain. Consider that the athermal component is a unique function of plastic strain at low test temperatures. That is, the stress-strain curves are in fact exactly parallel as the series of test temperature is lowered. This has been shown to be the case for a series of HSLA steels (Lucas and Gerberich, 1981). Thus by subtracting out the appropriate thermal component the strain-hardening portion remains, giving

$$\sigma_{i(\varepsilon_p)} = k_i \varepsilon_p^{\beta_i} \tag{7}$$

where the i's refer to the athermal or internal components. It follows from Eqs. (5) and (7) that

$$\partial\sigma/\partial\varepsilon_p = \beta k \varepsilon_p^{\beta-1} = \partial\sigma_i/\partial\varepsilon_p = \beta_i k_i \varepsilon_p^{\beta_i-1} \tag{8}$$

For any strain level, k and k_i may be described by Eqs. (5) and (7) in terms of the other parameters and eliminated from Eq. (8) giving

$$\beta\left\{\frac{\sigma_{(\varepsilon_p)}}{\varepsilon_p^{\beta}}\right\}\varepsilon_p^{\beta-1} = \beta_i\left\{\frac{\sigma_{i(\varepsilon_p)}}{\varepsilon_p^{\beta_i}}\right\}\varepsilon_p^{\beta_i-1}, \quad \text{or} \quad \beta = \frac{\beta_i \sigma_{i(\varepsilon_p)}}{\sigma_{(\varepsilon_p)}} \tag{9}$$

With Eq. (6), and dropping the subscripts, this becomes

$$\beta = \beta_i \sigma_i/(\sigma^* + \sigma_i) \tag{10}$$

Thus, in principle, if β_i and σ_i are determined at a temperature $T > T_c$ where σ^* is zero, then β should be predictable from Eq. (10) at any lower temperature or higher strain rate as long as $\sigma^*_{(T,\dot{\varepsilon})}$ is known.

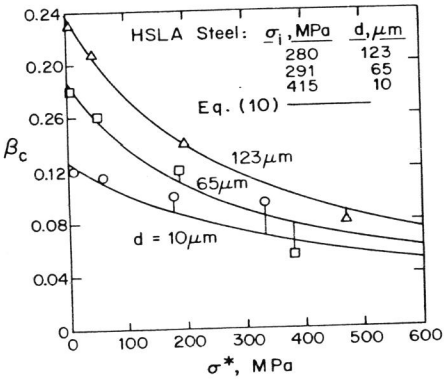

Fig. 3. Interrelationship between the strain-hardening exponent and the thermal component of the flow stress.

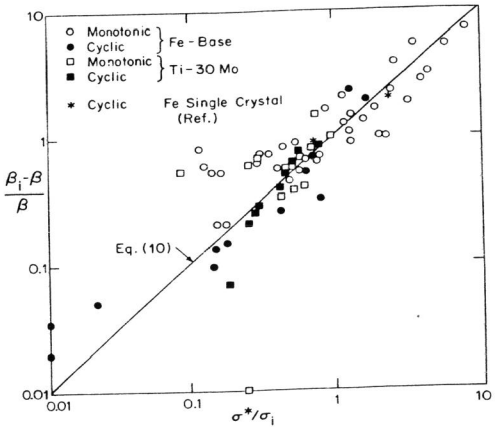

Fig. 4: Comparison of Eq. (10) to BCC metals and alloys.

To demonstrate the validity of this relationship, the values of β_i as previously determined to be 0.126, 0.184 and 0.238 for three HSLA steels (Lucas and Gerberich, 1981) having grain sizes of 10, 65, and 123 μm are treated. As seen in Fig. 3, the theoretical relationship of Eq. (10) predicts the cyclic strain-hardening exponents reasonably well at all other lower test temperatures. Similar predictive capabilities for static strain hardening behavior in Fe-binary alloys also has been shown (Gerberich, Nayar and Hayman, 1984). As a summary of these data, Eq. (10) should result in a linearly increasing plot of $(\beta_i-\beta)/\beta$ versus σ^*/σ_i. This relationship is seen to hold in Fig. 4. It is also important to demonstrate the relationship between β and the strain-rate sensitivity. Since $\beta_i\sigma_i$ is a mildly varying function of material alloy content (Yu, Esaklul and Gerberich, 1984) or grain size (Lucas and Gerberich, 1981) for this class of materials, it follows from Eq. (10) that $\beta \sim$ constant$/\sigma_{ys}$. Furthermore, it may be shown that the yield strength, for these materials, is approximately related to the strain rate sensitivity exponent, m^*, by the same constant, i.e. $\sigma_{ys} \sim$ constant m^*. Combining these two relationships,

$$\beta \text{ or } \beta_c \sim 1/m^* \qquad (11)$$

Within the scatterband of Fig. 5, this approximation is roughly followed. The purpose of this is to illustrate the dilemma with which one is faced when attempting to decide upon one of several models, e.g. where strain-rate sensitivity or strain-hardening might be controlling factors. These are discussed in detail in the Appendix where it is shown that such models might result in

$$\Delta K_{th} \propto (m^*+1)^{1/m^*} \qquad (12) \quad ; \quad \Delta K_{th} \propto (1/\sigma_{ys})^{[\beta_c+1]/[\beta_c+2]} \qquad (13)$$

It is best to provide an illustration where σ_{ys}, β_c and m^* have all been measured (Lucas, 1983). This is shown in Table 2 for HSLA steel. Comparing the last two columns, it is seen that the two scaling factors have the same trend and in fact display a linear regression correlation coefficient of 0.92. Although the implication is that threshold would decrease with decreasing temperature, this is more than offset by the strong temperature dependence of σ^* and σ_{ys} which appear separately in such models.

Table 2 Comparison of Strain-Rate Sensitivity and Strain-Hardening Parameters of Eqs. A-14 and A-19

HSLA steel	Temp., K	σ_{ys}, MPa	β_c	m^*	$(m^*+1)^{1/m^*}$	$(1/\sigma_{ys})^{\beta_c+1/\beta_c+2}$
10 μm	300	415	0.125	4.5	1.46	0.041
	233	463	0.120	6.0	1.38	0.039
	173	641	0.100	12.5	1.23	0.034
	123	827	0.095	21.0	1.16	0.030
65 μm	300	212	0.175	3.0	1.59	0.055
	233	269	0.160	3.5	1.54	0.050
	173	460	0.125	10.5	1.26	0.039
	123	650	0.055	18.0	1.18	0.036
123 μm	300	246	0.23	3.0	1.59	0.048
	233	278	0.205	3.0	1.59	0.046
	173	461	0.150	10.5	1.26	0.038
	123	649	0.075	18.0	1.18	0.035

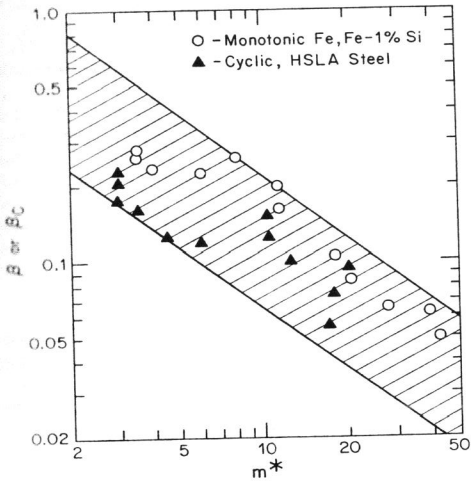

Fig. 5: Relationship between strain-hardening and strain-rate sensitivity exponents.

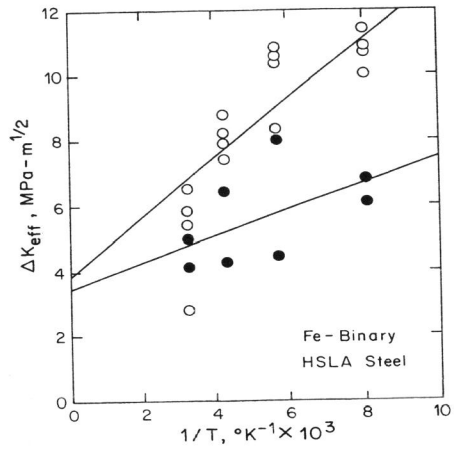

Fig. 6: The influence of decreasing test temperature on increasing ΔK_{eff}.

THRESHOLD MODELS

Consider the first contribution to threshold in Eq. (4), the effective value or that which remains after closure effects have been subtracted. To demonstrate the strong effect of test temperature on $\Delta K_{th(eff)}$, all data on Fe-Si binary alloys (Yu, Esaklul and Gerberich, 1984) and HSLA steels (Esaklul, Yu and Gerberich, 1984) are plotted in Fig. 6. For a given test temperature, there is considerable variation which is attributed to grain size, alloy content, yield strength and microstructural differences. Nevertheless, in both cases there is a dependence of test temperature on $\Delta K_{th(eff)}$ with lower temperatures producing higher thresholds. Clearly, this has to do with some thermally activated process. Whether this is largely the effect of test temperature on yield strength, strain-rate sensitivity or cyclic strain-hardening is not obvious. These parameters and their effect on $\Delta K_{th(eff)}$ are examined more closely in the following discussion. In section two of the Appendix, three threshold models for the effective stress intensity, $\Delta K_{th(eff)}$ are derived. The first two are in terms of dislocation dynamics. The later one is in terms of damage accumulation using the Manson-Coffin relationship. The purpose here was to present three models, one where the strain-rate sensitivity exponent, m^*, appeared, one where yield strength played the major role and one where the cyclic strain-hardening exponent, β_c, appeared. These three models give

$$\text{Model 1:} \quad \Delta K_{th(eff)} = \sigma^*\sqrt{2\pi L_s}\left\{\frac{2\omega L_s[m^*+1]\rho_m b}{\dot{\varepsilon}}\right\}^{1/m^*} \qquad (14)$$

$$\text{Model 2:} \quad \Delta K_{th(eff)} \simeq \sigma_{ys}\sqrt{12\pi L_s} \qquad (15)$$

$$\text{Model 3:} \quad \Delta K_{th(eff)} \simeq \sigma_{ys}\sqrt{12\pi}\, L_s^{1/2(\beta_c+2)}\left[\frac{da}{dN}\left(\frac{E}{\sigma_{ys}}\right)^2\right]^{(\beta_c+1)/2(\beta_c+2)} \qquad (16)$$

Model 1 may be considered as a true threshold below which no further crack advance would take place. Models 2 and 3 are apparent thresholds in that they are evaluated from crack growth laws at a measurement point of 10^{-10} m/cycle. In Figs. 7 and 8, these three models are compared to measured effective threshold stress intensities as defined by Eq. (3). These Fe-Si alloy data were collected at four test temperatures each ranging from 123 to 300 K (Yu, Esaklul and Gerberich, 1984). The parameters σ^*, L_s, m^*, ρ_m, b, $\dot{\varepsilon}$, β_c and σ_{ys} are described in the Appendix. In Fig. 7, the resulting fit is good for Eq. (14) but relatively poor for the approximation represented by Eq. (15). In Fig. 8, the resulting fit is probably the best of the three models. All of the parameters except ρ_m and L_s were measured independently in tensile tests. The mobile dislocation density, ρ_m, was estimated as $10^{14}/m^2$ and held constant for all alloys and test conditions. The one caveat is that cyclic β_c values were not available for Eq. (16) and so static strain-hardening values had to be utilized. The major fitting parameter common to all three models was L_s, the sub-cell spacing. However, to obtain a good fit, L_s had to be 45 μm for Model 1, 24 μm for Model 2 and 10 μm for Model 3. If one takes the more exact analysis of Eq. (A-5), the fit is achieved by taking L_s to be approximately 9 μm. Nevertheless, all of these values are too large since measured sub-cells at crack tips were in the vicinity of 1 to 5 μm (Davidson and Lankford, 1981).

This lack of agreement caused a reexamination of the threshold measurements with more sensitive instrumentation. The results, discussed in more detail in the next section, generally gave higher values of K_{op} and thus lower values of ΔK_{eff}. These are shown as the solid symbols in Fig. 8. In order to shift these points to the left on the abscissa of Fig. 8 so they fit Eq. (16), a new value of $L_s \sim 2$ μm was required. This is more realistic in terms of the measured sub-cells and gives additional weight to this model. It is clear that decreases in L_s for Models 1 and 2, although not as large, would also be achieved. Considering the approximations, the data scatter, and the ability to separate closure effects, one cannot say that any of these three models are best.

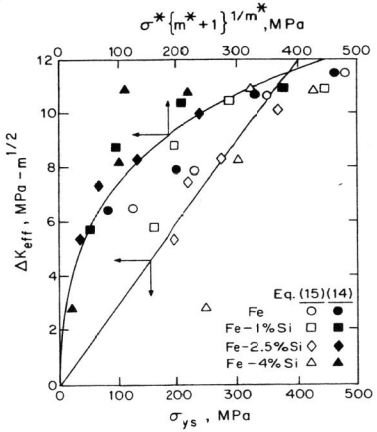

Fig. 7: Comparison of ΔK_{eff} to theoretical predictions of Eqs. (14) and (15).

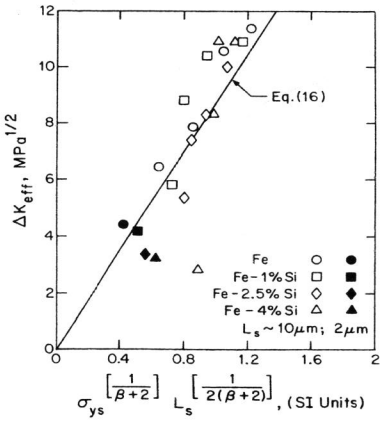

Fig. 8: Comparison of ΔK_{eff} to theoretical predictions of Eq. (16).

Closure Effects

For comparison to the $\Delta K_{th(eff)}$ data in Fig. 6, a similar plot for the closure contribution is shown in Fig. 9. Note that this is very similar to the effect of test temperature on $\Delta K_{th(eff)}$. Detailed discussion of reverse plastiticy, microgeometrical (e.g. asperities), and oxide-induced closure contributions are given elsewhere (Gerberich, Yu and Esaklul, 1984). It is sufficient to state that at low test temperatures this may be given by

$$K_{op}^2 \simeq \frac{\alpha' r^{1/2} \Delta K_{th} \sigma_{ys}}{(1-R)^2} + \frac{\alpha'' E d \sigma_{ys}}{1-R} \quad ; \quad (\Delta K/\sigma_{ys})^2 >> \frac{24r}{\pi} \qquad (17)$$

Here, R is the load ratio, r is the distance behind the crack-tip at which closure occurs, d is the grain diameter, α' is a constant and α" is $[1-\dot{\varepsilon}_{creep}\Delta t]$. It is seen that as ΔK_{th} increases with decreasing test temperature, K_{op} should increase as observed in Fig. 9. The $[1-\dot{\varepsilon}_{creep}\Delta t]$ term represents the creep of asperities during the contact closure time, Δt. That is, even though these tests were conducted at room temperature and below, the contact stresses of asperities are beyond yield and time-dependent creep occurs. To evaluate this, a series of tests were conducted at 300 K by reaching threshold under a standard load-shedding procedure and then intermittently remeasuring closure (Lei, Yu and Gerberich, 1984). The rest time between measurements was in the unloaded condition so that asperities could creep. In Fig. 10, the opening stress-intensity values as a function of time at rest are seen to first decrease and then increase. The initial decrease is consistent with the creep of asperities. The reversal was unexpected and was attributed to crack-tip relaxation processes which allowed sufficient crack advance on subsequent openings to allow a new set of asperities to contact. Although not completely definitive, the above observations are reasonable evidence that both reverse plasticity and geometric closure contributions of Eq. (17) are important ones. Additional evidence is given elsewhere (Beevers, 1982; Ritchie and Suresh, 1982; Esaklul, Wright and Gerberich, 1983).

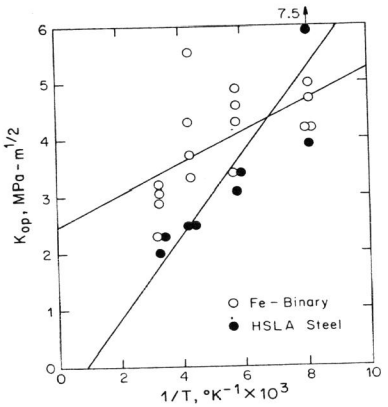

Fig. 9: The influence of decreasing test temperature on increasing K_{op}.

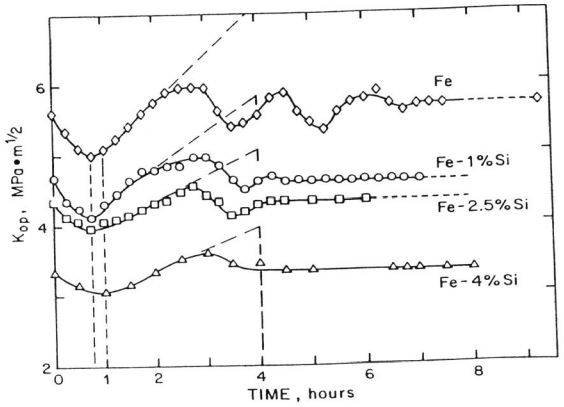

Fig. 10: The influence of time on K_{op}.

Synthesis of Threshold Contributions

It is apparent that there are major intrinsic $[\Delta K_{th(eff)}]$ and extrinsic $[K_{op}]$ contributions to threshold and that these are both affected by variations in test temperature. To combine these contributions, Eq. (14) of Model 1 was used to represent the effective contribution. It was simplified by representing $\sqrt{2\pi}\ \{2\omega L_s[m^*+1]\rho_m b/\dot{\varepsilon}\}^{1/m^*}$ as a constant, α'', which is reasonable at large m^* but underestimates the parameter by about a factor of two[2] at room temperature. By combining the modified Eq. (14) with Eqs. (4) and (17), a quadratic is obtained with two terms, not containing ΔK_{th}, of opposite sign. Eliminating those as second order effects, the final result is

$$\Delta K_{th} \sim 2\alpha'' \sigma^* \sqrt{L_s}(1-R) + \alpha' \sigma_{ys} \sqrt{r} \qquad (18)$$

It is interesting that although the physical interpretation of the two terms in Eq. (18) is substantially different, the form is nearly the same as Taira, Tanaka and Hoshina's (1979) and Yokobori and Yokobori's (1982) earlier models. The main difference here is that one term is a closure term as opposed to alternative explanations in the previous models. Taking $2\alpha'' \sqrt{L_s}$ to be 0.03 $m^{1/2}$, α' to be 2 and r to be associated with the ferrite grain size, the calculated threshold values are seen to give a narrow scatter band when compared to observed values in Fig. 11. The underprediction near room temperature may be attributed to the approximation used in Eq. (14). Using the same values for α'' and α' in Fig. 12 gives an equally good correlation for HSLA steel where R values were varied. The exceptions were for very coarse grained material tested at high R and low test temperature as represented by the solid circles. As discussed elsewhere (Esaklul, Yu and Gerberich, 1984) there is a mean stress effect on threshold in that high mean stress leads to high K_{max} which induces cyclic cleavage and reduces threshold. As this alternative fracture mode relationship is not built into the structure of Eq. (18), one would not expect

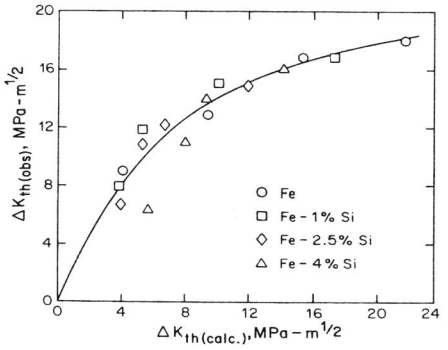

Fig. 11: Comparison of observed to calculated ΔK_{th} values for Fe-binary alloys using Eq. (18).

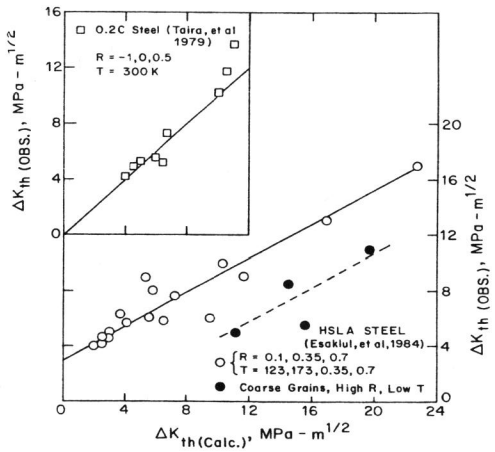

Fig. 12: Similar comparison for steels.

[2] Note that this underestimation is forced at room temperature because we are selecting a single value of α'' to represent all test temperatures. This would not be the case if only one test temperature were involved.

agreement. Finally, Eq. (18) is compared to Taira, Tanaka and Hoshina's data (1979) obtained at three different R values and three different grain sizes, all at room temperature. Using a single value of $2\alpha'' \sigma^* \sqrt{L_s}$ to be 4 MPa-$m^{1/2}$ and α' as before, Eq. (18) is seen to give an excellent fit to Taira, Tanaka and Hoshina's data. For this comparison, r was taken to be the grain size, for the three conditions of their study, which were 7.8, 20.5 and 55 μm having 366, 275 and 194 MPa yield strengths, respectively.

SUMMARY AND CONCLUSIONS

1. Fatigue threshold stress intensities increase substantially as test temperature is reduced from 300 to 123 K in Fe-base alloys.

2. Important contributions to threshold include both an intrinsic or effective threshold stress intensity $[\Delta K_{th(eff)}]$ and an extrinsic or opening stress intensity $[K_{op}]$.

3. At least three models give reasonable correlations to $\Delta K_{th(eff)}$ which are interpreted in terms of either strain-rate sensitivity, m^*, yield strength, σ_{ys}, or cyclic-strain-hardening, β_c, variables.

4. It is not clear what the best representation for $\Delta K_{th(eff)}$ is since β_c and m^* are interrelated, i.e. $\beta_c \sim 1/m^*$.

5. First order approximations which include $\Delta K_{th(eff)}$, K_{op} and load ratio effects, give reasonable correlations to observed thresholds but are not definitive with regards to controlling mechanism(s).

ACKNOWLEDGEMENTS

This work was supported by the Division of Materials Science of the Basic Energy Sciences Division of the Department of Energy under Contract DOE/DE-AC02-79ER10433.

REFERENCES

Antolovich, S., Saxena, A. and Chanani, G. (1976), Engng. Fract. Mech., 7, 649.
Beevers, C. (1982). In D. Francois (Ed.), Advances in Fracture Research, 3, ICF 5, Pergamon Press, New York, p. 1335.
Burck, L. and Weertman, J. (1976), Met. Trans., 7A, 257.
Davidson, D. and Lankford, J. (1981), Int. J. Fracture, 17, 257.
Esaklul, K., Wright, A. and Gerberich, W. (1983), Scripta Met., 17, 1073.
Esaklul, K., Yu, W. and Gerberich, W. (1984). In R. Stephens, W. Gerberich, R. Tobler and D. Pettit (Eds.), Fatigue at Low Temperatures, ASTM, in press.
Gerberich, W., Yu, W. and Kurman, E. (1983). In E. C. Aifantis and J. P. Hirth (Eds.), Int. Symp. on the Mechanics of Dislocations, in press.
Gerberich, W., Yu, W. and Esaklul, K. (1984) Met. Trans., 15A, No. 5, in press.
Gerberich, W., Nayar, A. and Hayman, C. (1984) unpublished data.
Lei, M., Yu, W. and Gerberich, W. (1984), Fatigue of Engng, Mat'ls and Structures, in press.
Lucas, J. and Gerberich, W. (1981), Scripta Met., 15, 327.
Lucas, J. (1983) Ph.D. Thesis, University of Minnesota, Minneapolis.
Masounave, J. and Bailon, J. (1976), Proc. 2nd Int. Conf. on Mech. Beh. of Mat'ls, ICMII, ASM, Metals Park, OH, p. 636.

Mughrabi, H., Herz, K. and Stark, X. (1976) Acta Met., 24, 659.
Ritchie, R. and Suresh, S. (1982) Met. Trans., 13A, 937.
Sadananda, K. and Shahinian, P. (1977), Int. J. Fract., 13, 585.
Taira, S., Tanaka, K. and Hoshina, M. (1979). In J. Fong (Ed.), Fatigue Mechanisms, ASTM STP 675, Am. Soc. Tst. Mat'ls., p. 135.
Yokobori, A. Jr., and Yokobori, T. (1982). In A. Blom and C. Beevers (Eds.), Fatigue Thresholds, 7, EMAS, p. 171.
Yu, C. and Yan, M. (1980), Fatigue of Engng. Mat. and Structure, 3, 189.
Yu, W. and Gerberich, W. (1983), Scripta Met., 17, 105.
Yu, W., Esaklul, K. and Gerberich, W. (1984), Met. Trans., 15A, in press.
Weiss, V. and Lal, D. (1974), Met. Trans., 5, 1974.

APPENDIX

Comparison of Strain-Rate Sensitivity and Strain-Hardening Contributions to Threshold

To accomplish this, we use models to be derived in the next section. From Eqs. A-4 and A-9, it is seen that these give

$$\Delta K_{th(eff)} \propto \sigma^* \left\{\frac{2\omega L_s \rho_m b}{\dot{\varepsilon}}\right\}^{1/m^*} \{m^*+1\}^{1/m^*}$$

$$\Delta K_{th(eff)} \propto \sigma_{ys} \left\{\frac{da}{dN} E^2\right\}^{(\beta_c+1)/2(\beta_c+2)} \left\{\frac{1}{\sigma_{ys}}\right\}^{(\beta_c+1)/(\beta_c+2)}$$

Since, for this investigation, $\sigma^*\{2\omega L_s \rho_m b/\dot{\varepsilon}\}^{1/m^*}$ scales closely to yield strength and $(da/dN)E^2$ is numerically equal to unity, only the last term in brackets in each equation is relevant. These terms represent Eqs (12) and (13).

Effective Threshold Criteria, $\Delta K_{th(eff)}$

Three possible threshold models are given here, the first in terms of a true threshold where no crack movement would be expected and the last two in terms of an apparent threshold where cracks may be slowly growing.

Dislocation travel time from crack-tip to cell wall. The first model is in terms of dislocation destabilization of a cell-wall structure and is described in more detail elsewhere (Gerberich, Yu and Kurman, 1983). The mechanics are essentially the same as has been developed by Yokobori and Yokobori (1982) but the substructural details are different. Basically, the picture is a crack-tip emitting a dislocation with the travel time to the next dislocation cell wall being the critical event. This is shown schematically in Fig. A-1 for

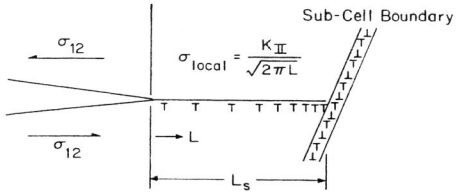

Fig. A-1: Threshold model in terms of a dislocation pile-up interacting with the sub-cell dislocation structure. Mode II depiction.

mode II cracking. In the more detailed treatement, it is demonstrated by computer simulation that a relatively small dislocation pile-up at a tilted sub-cell wall may destroy it. It is proposed that once the cell wall is destroyed, the long-range back stress decreases and the crack advances to a new equilibrium position. The controlling features are the sub-cell wall spacing, L_s, and the dislocation velocity. With constant stress rate testing in a triangular wave form, an emitted superdislocation arrives at the sub-cell boundary in time,

$$t_{L_s} = \frac{K(t_{L_s})}{2\omega K_{max}} \qquad (A\text{-}1)$$

where ω is the test frequency and K_{max} is the maximum stress intensity value in the stress cycle. Using a dislocation velocity relationship, $v = v_o(\sigma^*/\sigma_o)^{m^*}$, and the mean value theorem at a distance, L_s, from the crack tip gives the average velocity at L_s during the fatigue cycle to be

$$\bar{v} = \frac{v_o}{m^*+1}\left(\frac{K_{L_s}}{\sqrt{2\pi L_s}\,\sigma_o}\right)^{m^*} \qquad (A\text{-}2)$$

It is known that the superdislocation would slow in the vicinity of the cell-wall due to the back stress and the further distance from the crack tip. Although not exact, an assumption is that the controlling velocity is the average velocity at L_s. With this and the fact that $t_{L_s} \sim L_s/\bar{v}$, a first order estimate from (A-1) and (A-2) gives

$$t_{L_s} \simeq \frac{L_s(m^*+1)}{v_o}\left[\frac{\sqrt{2\pi L_s}\,\sigma_o}{2\omega K_{max} t_{L_s}}\right] \qquad (A\text{-}3)$$

It is interesting that this pedagogical model, except for a constant on the order of unity, gives the result obtained by Yokobori and Yokobori (1982) using group dislocation dynamics. Since $\Delta K_{th(eff)} = K_{max}$ at $R = 0$, for no closure effects, and $t_{L_s} = 1/2\omega$ for a triangular wave form at threshold, Eq. (A-3) may be written as

$$\Delta K_{th(eff)} = \sigma^*\sqrt{2\pi L_s}\left\{\frac{2\omega L_s[m^*+1]\rho_m b}{\dot{\varepsilon}}\right\}^{1/m^*} \qquad (A\text{-}4)$$

where ρ_m is the mobile dislocation density and $\dot{\varepsilon}$ is the strain-rate at which ρ_m, σ^* and m^* were determined in a tensile test (Yu, Esaklul and Gerberich, 1984). The elimination of σ_o was achieved by using $\sigma_o = \sigma^*(\rho_m b v_o/\dot{\varepsilon})^{1/m^*}$ from the dislocation velocity relationship. Note that Eq. (A-4) becomes Eq. (14).

Measurement point definition of threshold from dislocation dynamics. In a more practical sense, it may be that for some materials, that fatigue cracks nearly always grow if closure is absent. A practical treatment is similar to what has been done for the fatigue limit in face-centered-cubic materials where an arbitrary definition of endurance limit is made at 10^8 cycles. Similarly, if an arbitrarily small crack advance of 1 mm is assumed to represent no danger to design estimates, then a da/dN of 1 mm/10^8 cycles or 10^{-11} m/cycle would represent a "threshold" in these materials. It has been more typical to use 10^{-10} m/cycle to define thresholds in the laboratory and so we will use the later value. Such an analysis recently made and applied to Fe-base alloys at low temperatures was evaluated at high values of the strain-rate sensitivity exponent (m^*) which occur at low temperatures. It is derived elsewhere (Yu,

Esaklul and Gerberich, 1984) that the effective stress intensity may be described by

$$\Delta K_{th(eff)} = \sqrt{12\pi L_s}\left[\frac{\sigma_i + \alpha_1 \sigma^* \gamma_o^{1/m^*}}{\sigma_{ys}^{1-2\beta'}}\right]^{1/2\beta'}, \text{ with} \qquad \text{(A-5)}$$

$$\alpha_1 = \left(\frac{da/dN}{\Theta\, \Omega_1}\right)^{2/m^*} \; ; \quad \gamma_o = \frac{\phi \rho_m b v_o}{\dot{\varepsilon}} \; ; \quad \Omega_1 = \frac{1-\nu^2}{E}\left[\frac{v_o}{2(m^*+1)\omega}\right]^{1/2} \; ; \quad \beta' = \frac{m\beta+1}{m(\beta+1)}$$

Here, da/dN is taken as the measurment point of 10^{-10} m/cycle $\Theta \sim 1$, ρ_m is the mobile dislocation density taken to be $10^{14}/m^2$, $\dot{\varepsilon}$ is the tensile test strain rate of $8.3 \times 10^{-4} s^{-1}$, v_o is 0.01 m/s, b is the Burgers vector, and ϕ is 0.5. For the materials and test temperatures of interest, a first-order simplification may be made since $\alpha_1 \gamma_o^{1/m^*}$ ranges from 0.93 to 1.2 and thus may be taken as unity. Since $(\sigma_i + \sigma^*)$ is the yield strength, σ_{ys}, Eq. (A-5) becomes

$$\Delta K_{th(eff)} \simeq \sigma_{ys}\sqrt{12\pi L_s} \qquad \text{(A-6)}$$

which is Eq. (15) in the text. Note the similar form of this and Eq. (2b).

Measurement point definition of threshold using damage accumulation. Antolovich, Saxena and Chanani (1976) have described the average plastic strain in a region, Δa, at the crack tip and related it to the reverse plastic zone, giving

$$R_{P_\pm} = \frac{\bar{\varepsilon}_p}{0.7}\frac{\Delta a}{\sigma_{ys}} \qquad \text{(A-7)}$$

Relating the average plastic strain to the local reverse plastic strain, $\Delta\varepsilon_p^{local}$, and using the incremental number of cycles to accumulate damage in this region, i.e. the Manson-Coffin relation, $\Delta N \sim (\varepsilon_f/\Delta\varepsilon_p^{local})^2$, one finds

$$\frac{da}{dN} \simeq \frac{\Delta a}{\Delta N} \simeq 0.7\, R_{P_\pm}\frac{\sigma_{ys}}{E}\frac{\Delta\varepsilon_p^{local}}{\varepsilon_f^2} \qquad \text{(A-8)}$$

Using a strain distribution of $(\sigma_{ys}/E)(R_{P_\pm}/r)$ and a reverse plastic zone as is used in Eq. (2a), one can derive from Eqs. (A-7) and (A-8) that for $\varepsilon_f \sim 1$,

$$\text{Model 3:} \quad \Delta K_{th(eff)} \simeq \sigma_{ys}\sqrt{12\pi}\, L_s^{1/2(\beta_c+2)}\left[\frac{da}{dN}\left(\frac{E}{\sigma_{ys}}\right)^2\right]^{(\beta_c+1)/2(\beta_c+2)} \qquad \text{(A-9)}$$

which is Eq. (16) in the text. Here β_c is the cyclic strain-hardening exponent and da/dN is taken as 10^{-10} m/cycle as before.